Drilling oil-based mud waste as a resource for raw materials: a case study on clays reclamation and their application as fillers in polyamide 6 composites.

SIDDIQUE, S., LEUNG, P.S. and NJUGUNA, J.

2021

Drilling Oil-Based Mud Waste as a Resource for Raw Materials: A Case Study on Clays Reclamation and Their Application as Fillers in Polyamide 6 Composites

Shohel Siddique[1], Pak Sing Leung[2] and James Njuguna[1*]

[1]Centre for Advanced Engineering Materials, School of Engineering, Robert Gordon University, Riverside East, Garthdee Road, Aberdeen, AB10 7GJ, UK

[2]Department of Mechanical and Construction Engineering, Northumbria University, Ellison Place, Newcastle upon Tyne, NE1 8ST, UK

Corresponding Author Email : j.njuguna@rgu.ac.uk; Tel. +44 (0) 1224262304

Abstract

To convert the hazardous oil-based mud waste into a resource, this study has addressed reclaimed nanoclays and its application as a filler material for reinforcing polyamide 6 polymer matrix into a novel polymer composite material. This work focuses on the synergistic effect of complex mixture of various clay minerals reclaimed from oil-based mud waste on different mechanical properties in polyamide-6 (PA6)/oil-based mud fillers (OBMFs) nanocomposites. PA6/OBMFs nanocomposites were manufactured through the melt compounding of OBMFs with PA6 in a twin-screw extruder followed by injection moulding.

The study shows significant improvement for mechanical properties. For instance, the tensile properties increased with the incremental loadings of OBMFs in PA6

matrix. The Young's moduli were increased by 42% and 35% in PA6 with 7.5 and 10 wt% OBMFs nanocomposites respectively whereas the tensile strengths were increased by 24% and 16% in PA6 with 7.5 and 10 wt% OBMFs nanocomposites respectively. The flexural strength increased by 26% with the addition of OBMFs from 0 to 10 wt% in PA6. The storage modulus of the nanocomposite containing 10 wt% OBMFs was 16% higher than the storage modulus of neat PA6 at 30° C, whereas at 60° C (glass transition temperature, T_g of neat PA6) the storage modulus of PA6 with 10 wt% OBMFs was 56% higher than that of neat PA6. The study shows that the oil-based mud waste can be appropriately management to develop a new raw materials resource for polymer technology.

Keywords: Drilling Oil-Based Mud Waste, nanoclay, polyamide 6, drilling waste management, nanocomposites, mechanical properties

Graphic abstract

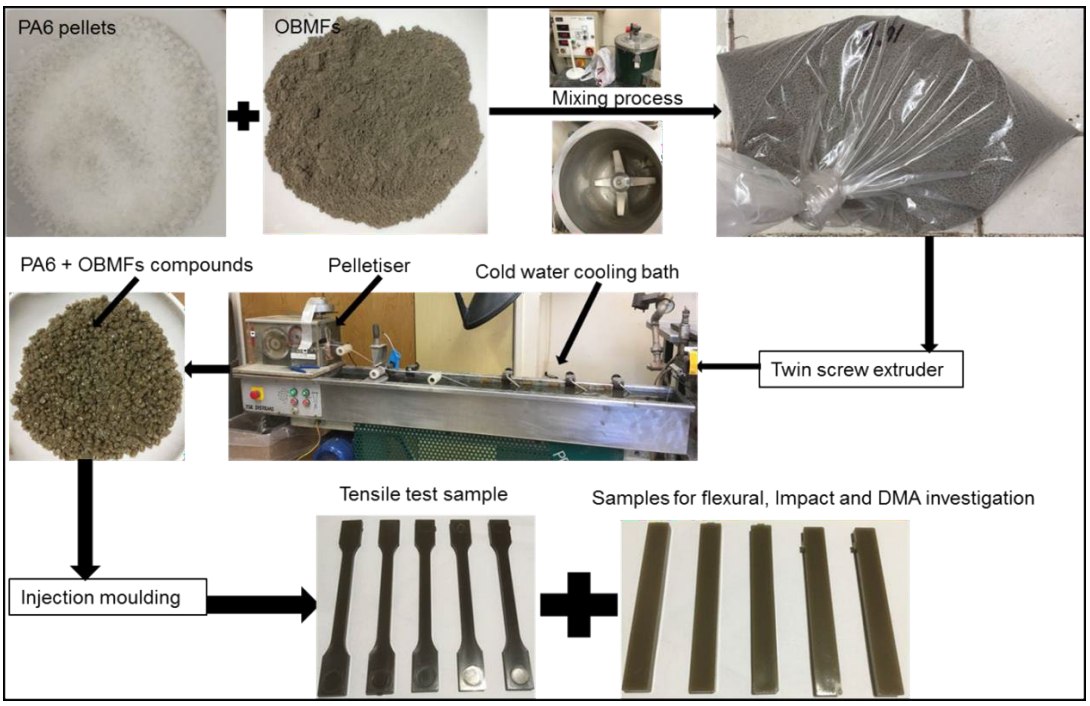

1. Introduction

Spent drilling mud, drill cuttings and adhered oils are the key target ingredients to deal with drilling waste treatment operations in oil and gas exploration industry (Tuncan *et al*., 2000, Arce-Ortega *et al*., 2004, Davarpanah *et al*., 2018 and Aftab et al., 2020). In early oil and gas operation industry, drilling wastes were discharged after the drilling operation directly to the landfill site or ocean which caused serious environmental pollution to the dumping site and its surrounding zones (Muschenheim and Milligan, 1996, Sadiq and Hussain, 2005 and Sadiq *et al*., 2003). In 2008, the Waste Framework Directive 2008/98/EC, identified and declared certain specific ingredients in drilling mud waste as hazardous chemicals for the sake of environmental pollution control measures (Siddique *et al*., 2017 and Chen *et al*., 2007). However, since the European Union (EU) Waste Framework Directive (WFD) in operation, drilling waste now cannot be disposed to landfill without different levels of treatment to meet the threshold limit of different chemicals including oil content and salinity to dispose to the landfill site (Robinson *et al*., 2009, Kogbara *et al*., 2016).

Historically, a wide range of treatment and disposal options are in practice now. However, a technical advancement of process optimisation to intensify the recycling and recovery of resources becomes an interesting area of research recently (ball *et al*., 2012, Ayati *et al*., 2019, Foroutan *et al*.,2018 and Siddique *et al*., 2020). Although the separated liquids (water and oil condensates) are currently being reused in drilling mud preparation and in some cases, the oil is utilised to provide power for the other equipment on the platform, it is important to note that, well conditions may vary and thus further analysis may be required to determine safest recycle or disposal

options (Ormeloh, 2014, Thermtech, 2012). In addition, there may be the need for supplementary treatment due to the heavy metal and large amount of salts present in the original drilling waste in certain cases (Holdway, 2002, Xu *et al*., 2018). This is imperative especially concerning the produced solids, which are currently being disposed off at landfill sites or recycled in the construction industry which may cause a serious threat to human life (El-Mahllawy and Osman, 2010, Pamukcu *et al*., 1990). Thermomechanical cuttings cleaner (TCC) is an example of the state-of-the-art technology for treating the drilling waste and its leaves solid residue that is still unfortunately disposed off into landfill sites (Thermtech, 2012).

Previous studies by Adegbotolu *et al*., (2014) and Siddique *et al*., (2018, 2019a, 2019b) focused on using the produced solids as reinforcement for polymer composites. However, this research delves further by assessing and improving on the operating mechanism of the TCC to efficiently produce the mineral powders (nanoclay) needed for use in the nanocomposite material industry. This will minimize the volume of drilling wastes disposed off at landfill sites and play a major role in reducing the carbon footprint of the oil and gas industry too.

Polymer/montmorillonite (MMT) nanocomposites become an interesting area of research since Toyota group first successfully developed PA6/MMT nanocomposites in 1987 (Choi *et al*., 2001, Huskić and Žigon, 2007, Ma *et al*., 2003). Since 1987 numerous reports have been published and claiming the improvements of different properties of material including increased stiffness and strength (Shah *et al*., 2016, Zare *et al*., 2019), improved thermal stability (Leszczyńska *et al*., 2007, Davis *et al*.,

2004, Lakshmi *et al*., 2008), reduced flammability (Qin *et al*., 2004, Li *et al*., 2009), improved chemical and solvent resistance (Wang *et al*., 2012, Huang *et al*., 2001), enhanced energy absorption (Sun *et al*., 2009, Silva *et al*., 2013) and augmented gas barrier properties (Priolo *et al*., 2011, Kalendová *et al*., 2013) by reinforcing only a few percent of MMT platelets in polymer matrix. MMT platelets are generally tightly stacked together due to the strong electrostatic forces between them and inhibit them to easily exfoliate in most polymers due to the incompatible nature of chemical features between MMT and polymer matrix surfaces (Zheng *et al*., 2004, Xie *et al*., 2001, Liu 2007).

Cation exchange surfactants were generally employed to modify the MMT surfaces to enhance the wettability of MMT platelets in the polymer matrix (Xi *et al*., 2005, Singla *et al*., 2012, Xi *et al*., 2007, Vazquez *et al*., 2008). Many articles claim the importance of organic modification of clay predominantly MMT surfaces and the role of processing (Mishra *et al*., 2012, Tjong *et* al., 2002, Meera *et al*., 2012). Shishan *et* al., (2004) reported that the modulus, bending strength and heat distortion temperature of PA6/MMT nanocomposites increased with increasing clay content but decreased the tensile strength with the addition of MMT more than 4.3 wt%. Tjong and Bao (2004) highlighted the improved strength and the stiffness of PA6/MMT nanocomposites at the expense of tensile ductility.

The bulk mechanical properties were studied by Liu *et al*., (2011) that PA6 with 3 wt% MMTs exhibited the best performance in tensile strength and flexural strength. It was also found in their study that higher loading of MMT in PA6 matrix-initiated agglomeration and leading to a decrease in tensile and flexural strength tests. Borse and Kamal (2006) presented the effect of different organophillic treatment of MMT surfaces, residence time and mixing efficiency during extrusion

process on mechanical properties of PA6/clay nanocomposites. Interesting findings were highlighted in their report that longer residence time and higher mixing efficiency during extrusion process produced the highest degrees of exfoliation and enhanced the mechanical properties of PA6/clay nanocomposites.

In our previous work Siddique *et al*., (2017, 2018, 2019a, 2019b), detailed investigations were completed based on the morphological, structural and thermal degradation study of heat treated reclaimed nanoclay reinforced PA6/OBMFs nanocomposites. The present work is an extension of previous study showing the influence of this novel filler in different mechanical properties of PA6/OBMFs nanocomposites.

2. Experiments

2.1. Materials

The PA6 used in this study has a melting point of 220°C, relative viscosity of 2.7±0.10, density 1.13 g/cm^3, cylindrical chip shape and chip size is 2.5 mm. the spent OBM slurry was supplied in kind by a local oil and gas service company in Aberdeen, United Kingdom. A comprehensive study on the characterisation of OBMFs including elemental and compounds composition of OBMFs and reported in Siddique et al 2020c and Siddique *et al* 2018). The recovered elements present in OBM waste sample analysis performed only when the r^2 of the calibration curve was higher than 0.999. The concentrations of alkaline earth metals (Mg, Ca, Ba), alkali metals (Na, K), transition metals (V, Cr, Mn, Fe, Ni, Cu, Zn, Cd), post-transition

metals (Al, Pb), metalloids (Si, As), polyatomic non-metals (P, S), and actinide (U) in the extracts were determined by using inductively coupled plasma optical emission spectrometry (ICP-OES) (Siddique *et al* 2018).

The thermo-chemical characteristics of OBM waste has confirmed that the presence of different clay minerals such as montmorillonite, halloysite, kaolinite and vermiculite including inorganic salts in OBM slurry powder (Siddique et al 2020c). The microscopic analysis revealed that the distance between polymer matrix and OBM slurry filler is less than that of widely used and commercially available montmorillonite, which suggests better interfacial adhesion of OBM slurry compared with the adhesion between montmorillonite and polymer matrix. This was also confirmed by X-ray diffraction (XRD) analysis which showed superior delamination structure OBM slurry compared with the structure of MMT. The presence of different clay materials such as montmorillonite, halloysite, kaolinite, vermiculite etc are established interesting clay materials to improve mechanical, thermal, gas and water barrier and flame- retardant properties of polymer composite material (Leszczyńska *et al*, 2007a, 2007b).

2.2. OBMFs manufacturing process

OBMFs manufacturing from OBM waste is described in detail in our previous works (Siddique *et* al., 2019a, Siddique *et* al., 2019b, Siddique *et* al., 2020c). For completeness, the filler manufacturing process is briefly described here stating the thermal treatment process of OBM waste where heat applied intermittently. In first

stage heat was applied for 12 hours remaining the temperature at 50°C. The oil content on the top surface was decanted and heated subsequently another 12 hours leaving the constant temperature at 80°C. The thick oil content on the top surface was decanted again before applying heat to maintain temperature at 700°C for 12 hours. The dry solid clay residue was crushed to produce fine clay filler using an ball mill.

2.3. PA6/OBMFs nanocomposite manufacturing process

To investigate the effect of reclaimed clay from spent OBM waste in Influencing different mechanical properties of PA6/OBMFs nanocomposites, PA6 was melt compounded with different amount (wt%) of Oil Based Mud fillers (OBMFs) such as 2.5, 5, 7.5 and 10 wt%. The manufacturing process of PA6/OBMFs nanocomposites was reported in our previous published paper (Siddique *et al.*, 2019a). However, the manufacturing process is briefly mentioned here. Prior to manufacture PA6/OBMFs nanocomposites, PA6 pellets and OBMFs were dried separately at 90° C for 24 hours in a convection oven before OBMFs was mixed in PA6 pellets to manufacture PA6/OBMFs nanocomposites. The mixture of PA6 and OBMFs in specific wt% loadings was then run through the co-rotating twin screw extruder at 250° C which was attached to the pelletiser at the end to cut the compounds into small pieces.

The obtained compound pellets were stored in thermally insulated bags for storing the compounds and protecting from absorbing moisture from air. These compounds were used to manufacture tensile, flexural and impact test bars using injection

moulding machine. Before using compounds to manufacture different test bars, compounds were dried at 90° C for 12 hours in a convection oven to ensure the effect of moisture in test results are as little as possible. The test bars were stored in two layers of aluminium foil followed by polythene zip bags for moisture absorption protection before performing the mechanical tests.

2.4. Testing and characterisation

The morphology observations of different platelets in OBMFs and the physical interaction including dispersion mechanisms of OBMFs with PA6 matrix were investigated using a Scanning Electron Microscope. The samples were gold coated using sputter deposition for 2 minutes before performing the analysis. The applied accelerating potential was 5.0 kV, leaving 8.0 mm the working distance and adjusting the magnification of 2000X. The nanomorphology, structure and thermal degradation behaviour have been reported in our previous work, Siddique *et* al., 2019a.

Tensile tests were performed according to the EN ISO 527 standard on a universal testing machine. The gauge length of test specimens was 80 mm and the applied test speed was 2 mm/min. the test process including elongation was monitored by video extensometer to acquire data to determine tensile properties of samples. The three point bending tests were performed according to the EN ISO 178 standard on a universal testing machine. The span length for the tests was 64 mm and the test speed of 2 mm/min according to the test instruction mentioned in the standard.

Dynamic mechanical analysis (DMA) was performed using DMA 8000. The sample dimension was 11.5mm X 10 mm X 4 mm and the testing temperature ranged from 25° C to 70° C at the temperature ramp of 2° C/ min.

The Charpy impact test is a versatile method for evaluating the fracture behaviour of polymeric materials at high strain rates due to the simplicity and convenience of the test. The test equipment setting and the sample preparation process in this study is described in previous section and illustrated in **Fig. S1 (in supplementary information)**. The Charpy impact tests were performed according to the EN ISO 179 standard with a on a Impactor instrument. The energy absorption of materials was analysed using both notched and un-notched specimens. The specification for notch samples was '~~A'~~ type with a radius of 0.25 mm notch tip, 45° angle and 2 mm depth. The dimension of cross section of the notched specimens was 4X8.1 ± 0.5% variance and the dimension of cross section of un-notched specimens was 4.01X9.9 ± 0.4% variance among different samples. The energy absorbed by the sample was recorded during test and impact strengths α_{cU} and α_{cN} were calculated with the following equation (Deák *et al*., 2010)]:

$$\alpha_{cU} \text{ or } \alpha_{cN} = \frac{Ec}{h.w} . 10^3 \qquad (1)$$

Where E_c is the energy absorbed by the tested sample, h is the thickness and w is the width of the samples. For notched test, w is the residual width of the samples.

3. Results and discussion

3.1. Morphology of PA6/OBMFs nanocomposites

The morphology investigation to identify the difference in OBMFs dispersion in PA6 matrix and micromechanical deformation behaviour among different nanocomposites is obvious from SEM observations of fractured surfaces in Fig. 1. A lesser extent of plastic deformation is noticeable in nanocomposites with 7.5 and 10 wt% OBMFs contents in comparison with neat PA6 matrix and nanocomposites with 2.5 and 5 wt% OBMFs loadings. For the PA6/OBMFs nanocomposites specimens studied at room temperature, significant particles dictating dispersion characteristics showed in Fig. 1.

[Fig. 1]

The morphology of OBMFs is presented in Fig. 1(a) which illustrates the shape and size of clay platelets present in OBMFs. The fracture surface in PA6 matrix demonstrates elastic deformation in Fig. 1(b) and is different from brittle fracture surfaces of PA6/OBMFs nanocomposites in Fig. 1(c-f). However, the matrix was plastically deformed due to addition of OBMFs in matrix and the degree of plastic deformation increased with the increase of OBMFs contents in PA6 matrix. The elastic deformation in some parts of samples is visible in Fig. 1(c) and 1(d) where clay platelets were closely embedded in matrix. The matrix/OBMFs adhesion was much stronger in Fig. 1(e) and 1(f) such that the clay particles had to break instead of just pulling out of the matrix. This explains the mechanisms of possessing higher tensile strength and Young's modulus of OBMFs reinforced polyamide while observing the tensile test.

3.2. Tensile properties of PA6/OBMFs nanocomposites

In this study, tensile properties of polyamide-6/OBMFs nanocomposites were investigated. Nanocomposite materials were manufactured and a set of five samples for each material were tested which are shown in Fig. 2(b-f) and neat polymer on Fig 2a. The average data is considered to identify different mechanical properties of each material.

[Fig. 2]

Fig. 2(b-f) presents the plastic deformation of materials by observing the colour changes in sample while the sample was under stress during tensile test. **Fig. S2** (in supplementary information) illustrates the tensile stress vs tensile strain curves for PA6/OBMFs nanocomposites.

The materials showed an incremental brittle behaviour without yield point which are observed in Fig. 2 (b-f) and stress-strain curves in **Fig. S2**. It can be observed that the Young's modulus was improved with the OBMFs loading from 0 to 10 wt% in **Fig. S2**. On the other hand, the deformation failure at lower stress and strain values are increases as the filler concentration decreases from 10 to 0 wt% (neat PA6) which is highlighted in Fig. 3.

[Fig. 3]

This deformation characteristic indicates the improvement in brittleness in nanocomposites due to the OBMFs reinforcement in PA6 matrix which is also reported by several authors in their investigations of clay addition in polymer matrix

(Gabr and Uzawa, 2018 and Liu *et al*., 2003). These results can be explained by the relation highlighted in our previous report Siddique el *et al*., (2019a, 2019b) where the effect of OBMFs loadings on structural and dispersion characteristic has been presented. It was found in that previous study that 2.5 and 5 wt% of OBMFs loadings in PA6 matrix showed exfoliation of OBMFs in PA6 matrix whereas 7.5 wt% of OBMFs in PA6 matrix showed intercalation of OBMFs platelets and 10 wt% OBMFs loading in PA6 matrix resulting agglomeration of OBMFs in PA6 matrix. A comparison of Young's modulus and tensile strength results of neat PA6 and PA6/OBMFs nanocomposites were highlighted in **Fig. S2** (in supplementary information) indicates that the larger the diameter of OBMFs, the stress concentration factor is lower, but the maximum stress acts when the cross-sectional area of filler increases.

Based on this argument, the superior Young's Modulus and tensile strength can be explained when OBMFs were intercalated and agglomerated in PA6 with 7.5 and 10 wt% OBMFs nanocomposites respectively. The Yong's moduli were increased by 42% and 35% in PA6 with 7.5 and 10 wt% OBMFs nanocomposites respectively. In addition to Young's moduli, the tensile strength was increased by 24% and 16% in PA6 with 7.5 and 10 wt% OBMFs nanocomposites respectively. The relation between stress concentration and dispersion behaviour of OBMFs in PA6 matrix also helps to understand the reduction of percentage elongation among neat PA6 and PA6/OBMFs nanocomposites which is presented in Fig. 4.

[Fig. 4]

The percentage of elongation was decreased by 236% and 240% in PA6 with 7.5 and 10 wt% OBMFs nanocomposites respectively. The increase elongation value for 5 wt% when compared to other nanocomposites is associated with the threshold limit to initiate exfoliation as previously observed in our earlier study (Siddique *et al*., 2019a). Similarly, it was observed that 4.2 wt% of OBMFs loading is the threshold limit to initiate exfoliation of OBMFs nanoplatelets in PA6 matrix which also affect the elongation property of PA6 with 5 wt% OBMFs nanocomposites. As discussed in Siddique *et al*., 2019a, the sigmoidal curve of percentage filler weight loading relationship to the total immobilised fraction (TIF) is associated to the dispersion nature of clays in polymer matrices.

The fractured surfaces of the tensile samples tested at 23° C correspond to an increasing trend of brittle fracture of samples as the filler concentration increases which is presented in Fig. 2(b-f). Fig. 2(b-f) illustrates the decreasing tendency of plastic deformation in samples transforming ductile fracture of samples to brittle failure of samples due to increasing the filler concentration from 0 to 10 wt% of OBMFs in PA6 matrix. Observing different mechanical properties and failure behaviour of samples it can be highlighted that the brittleness property of samples increased with the increasing content of OBMFs loadings in PA6 matrix. It can also be highlighted observing the morphology and tensile test results that the distances among the OBMFs in PA6 matrix increase with the OBMFs loading from 0 to 10 wt% in PA6 matrix which hinders chain scission reflecting the mechanical properties and fracture behaviour of materials.

3.3. Flexural properties of PA6/OBMFs nanocomposites

In this study, flexural properties of polyamide-6/OBMFs nanocomposites were investigated. Nanocomposite materials were manufactured and a set of five samples for each material were tested which are shown in Fig. 5(b-f). The average data is taken into account to identify different mechanical properties of each material.

[Fig. 5]

To identify different flexural properties of neat PA6 and PA6/OBMFs nanocomposites, flexural stress-strain curves were presented in **Fig. S3** (in supplementary information).

Fig. S3 showed that PA6/OBMFs nanocomposites have a higher stress points in respect to the corresponding strain points. It is also noticeable that the gradient of stress-strain curve increases with the increase of OBMFs loadings from 0 to 10 wt%. In Fig. 6 the flexural strength and flexural modulus of neat PA6 and PA6/OBMFs nanocomposites is shown as a function of OBMFs loadings. The flexural strength and flexural modulus of PA6/OBMFs nanocomposites increase with the incremental OBMFs loadings from 0 to 10 wt% which is presented in Fig. 6.

[Fig. 6]

A sharp increasing trend in flexural strength and flexural modulus is presented in Fig. 6. The significant improvement in both flexural strength and flexural modulus is noticeable in PA6 with 7.5 and 10 wt% OBMFs nanocomposites. The flexural

strength increases by 26% with the addition of OBMFs from 0 to 10 wt% in PA6. However, PA6 with 10 wt% OBMFs shows a more than 30% higher flexural modulus than the one with a neat PA6 matrix.

3.4. Impact fracture toughness properties of PA6/OBMFs nanocomposites

The influence of OBMFs on the toughness of PA6/OBMFs nanocomposites were evaluated comparing to the toughness of neat PA6 matrix. The toughness of both notched and un-notched neat PA6 and PA6/OBMFs nanocomposites samples is plotted against OBMFs contents in Fig. 7.

[Fig. 7]

The toughness is distinctly enhanced at lower OBMFs contents up to 5 wt% for notched samples whereas there is not any significant change noticeable for un-notched samples. However, the toughness is drastically reducing for both notched and un-notched PA6/OBMFs nanocomposites samples with OBMFs loadings from 5 to 7.5 wt%. For both notched and un-notched samples, there is not any remarkable effect is noticed in samples with 7.5 and 10 wt% OBMFs content. Stress whitening can be readily noticeable in the impact specimens of various wt% of OBMFs reinforced PA6 nanocomposite samples which is presented in Fig. 8.

[Fig. 8]

For notched samples, the stress whitening can be clearly noticeable through the fracture surfaces of samples which is not apparent to the top surfaces of samples which matches the same observation reported by Tjong and Bao (2004). They reported the energy dissipation mechanisms in samples highlighting the changes in energy dissipation in different layers in samples. The dispersion characteristics of OBMFs platelets influence the yielding or deforming behaviour of PA6/OBMFs nanocomposites (Jahromi *et al*., 2016). Findings from the previous study (Siddique *et al*., (2019a), it is anticipated that the exfoliation of OBMFs platelets in PA6 with 2.5 and 5 wt% OBMFs increases the toughness of materials whereas the toughness of PA6 with 7.5 and 10 wt% OBMFs nanocomposites are severely reduced due to the intercalation and agglomeration of OBMFs platelets in PA6 matrix. However, among different wt% contents of OBMFs in PA6 matrix, the impact strength of exfoliated OBMFs reinforced PA6 (PA6 with 2.5 and 5 wt% OBMFs nanocomposites) were higher than that of intercalated and agglomerated (PA6 with 7.5 and 10 wt% OBMFs nanocomposites respectively) OBMFs in PA6 matrix.

3.5. Dynamic mechanical analysis of PA6/OBMFs nanocomposites

Fig. 9 shows the storage modulus as a function of temperature for the PA6/OBMFs nanocomposites.

[Fig. 9]

It is clearly evident that OBMFs increased the storage modulus of PA6 within the temperature range tested. This result agrees with the tensile and flexural tests, where at ambient temperature it is also increased gradually with the incremental

loading of OBMFs in PA6 matrix. The improvement in modulus of PA6/OBMFs nanocomposites is caused by the stiffness of the OBMFs layers and the constraining effect of OBMFs platelets on molecular motion of PA6 chains. However, observing Fig. 9 it can be highlighted here that the storage modulus of the nanocomposite containing 10 wt% OBMFs was 16% higher than the storage modulus of neat PA6 at 30° C, whereas at 60° C (glass transition temperature, T_g of neat PA6) the storage modulus of PA6 with 10 wt% OBMFs was 56% higher than that of neat PA6. It is also clearly noticeable that the storage modulus of PA6 with 2.5 and 5 wt% OBMFs nanocomposites were very close to that of neat PA6 which governs the exfoliation of OBMFs in PA6 matrix does not have any significant effect on storage modulus of nanocomposite materials whereas the intercalation (PA6 with 7.5 wt% OBMFs) and agglomeration (PA6 with 10 wt% OBMFs) of OBMFs in PA6 matrix significantly increase the storage modulus property of materials.

The loss modulus curves of neat PA6 and its nanocomposites are presented in Fig. 10.

[Fig. 10]

Observing the loss modulus curves of neat PA6 and its nanocomposites in Fig. 10, it can be articulated that there was not any significant change in loss modulus for PA6 with 2.5 and 5 wt% OBMFs nanocomposites compare to that of neat PA6. However, there were significant drop in loss moduli of PA6 with 7.5 and 10 wt% OBMFs noticed in Fig. 10 which indicates that PA6 with 7.5 and 10 wt% OBMFs showed higher viscosity compare to that of neat PA6 in the same temperature

profile. The relaxation peak of neat PA6 at 60° C shifted to higher temperature for PA6 with 7.5 (65° C) and 10 (above 70° C) wt% OBMFs nanocomposites.

Tan delta is the ratio of loss modulus to storage modulus which represents the damping properties of material. It is a way of measuring the energy dissipation of a material which identifies the energy absorbing characteristics of material. Fig. 11 shows the magnitude of dynamic loss increased with the incremental loading of OBMFs in PA6 matrix.

[Fig. 11]

When the OBMFs platelets exfoliate in PA6 polymer chain, it is believed that the smaller crystallites produce more interfacial area. The increase in interfacial area influences to increase the restraint of tie chains between crystallites which results the reduction in the alpha loss tangent peak and thus increase in T_g which also agrees with findings reported by Gendre *et* al., (2015) and Yu *et al.*, (2004). The tan delta curves between 60 to 70° C indicates the rubbery state of neat PA6 at this temperature range whereas the tan delta peak shifts to higher temperature for PA6 with 10 wt% OBMFs nanocomposite represents the enhancement of relaxation peak due to the agglomeration of OBMFs in PA6 matrix.

4. Conclusions

The effect of OBMFs addition in PA6 matrix in different weight percentage was studied by manufacturing several PA6/OBMFs nanocomposites using melt compounding process. Addition of OBMFs clearly increased Young's modulus and tensile strength with compromising reductions in ductility and fracture toughness of

PA6. Tensile testing shows that the tensile modulus and strength of PA6/OBMFs nanocomposites increase with the incremental loading of OBMFs in PA6 matrix. the observed high elastic modulus, tensile strength, flexural modulus and flexural strength were attributed to reclaimed OBMFs nanoclay aggregation which was confirmed microscopically. A potential correlation between the filler surface area governed by the dispersion and distribution features of OBMFs in PA6 matrix was observed and discussed. The storage modulus and loss modulus curves of DMA highlight information regarding the quality of interface exist between OBMFs and PA6 polymer chains. The peak height of *tanδ* reflects the close relationship with the mobility of PA6 molecular chain segments and OBMFs nanoclay platelets. The study shows that the reclaimed nano/clays have potential applications as a filler in PA6. These properties make OBMFs reinforced PA6 matrix as a suitable candidate in polymeric engineering nanocomposite materials which can be used in industry in all fields where environmentally toxic, expensive, non-recyclable or limited recyclable nanocomposites have gained attention.

References

Adegbotolu, U.V., Njuguna, J., Pollard, P. and Yates, K., 2014. Waste to Want: Polymer nanocomposites using nanoclays extracted from Oil based drilling mud waste. In IOP Conference Series: Materials Science and Engineering (Vol. 64, No. 1, p. 012023). IOP Publishing.

Aftab, A., Ali, M., Arif, M., Panhwar, S., Saady, N. M. C., Al-Khdheeawi, E. A., Mahmoud, O., Ismail, A.R., Keshavarz, A. and Iglauer, S. (2020). Influence of tailor-made TiO2/API bentonite nanocomposite on drilling mud performance: Towards enhanced drilling operations. Applied Clay Science, 199, 105862

Arce-Ortega, J.M., Rojas-Avelizapa, N.G. and Rodríguez-Vázquez, R., 2004. Identification of recalcitrant hydrocarbons present in a drilling waste-polluted soil. Journal of Environmental Science and Health, Part A, 39(6), pp.1535-1545.

Ayati, B., Molineux, C., Newport, D. and Cheeseman, C., 2019. Manufacture and performance of lightweight aggregate from waste drill cuttings. *Journal of cleaner production*, *208*, pp.252-260.

Ball, A.S., Stewart, R.J. and Schliephake, K., 2012. A review of the current options for the treatment and safe disposal of drill cuttings. Waste Management & Research, 30(5), pp.457-473.

Borse, N.K. and Kamal, M.R., 2006. Melt processing effects on the structure and mechanical properties of PA-6/clay nanocomposites. Polymer Engineering & Science, 46(8), pp.1094-1103.

Chen, T.L., Lin, S. and Lin, Z.S., 2007, January. An innovative utilization of drilling wastes as building materials. In E&P Environmental and Safety Conference. Society of Petroleum Engineers.

Choi, Y.S., Choi, M.H., Wang, K.H., Kim, S.O., Kim, Y.K. and Chung, I.J., 2001. Synthesis of exfoliated PMMA/Na-MMT nanocomposites via soap-free emulsion polymerization. Macromolecules, 34(26), pp.8978-8985.

Davarpanah, A., Razmjoo, A. and Mirshekari, B., 2018. An overview of management, recycling, and wasting disposal in the drilling operation of oil and gas wells in Iran. *Cogent Environmental Science*, *4*(1), p.1537066.

Davis, R.D., Gilman, J.W., Sutto, T.E., Callahan, J.H., Trulove, P.C. and Hugh, C., 2004. Improved thermal stability of organically modified layered silicates. Clays and Clay Minerals, 52(2), pp.171-179.

Deák, T., Czigány, T., Tamás, P. and Németh, C., 2010. Enhancement of interfacial properties of basalt fiber reinforced nylon 6 matrix composites with silane coupling agents. Express Polymer Letters, 4(10).

El-Mahllawy, M.S. and Osman, T.A., 2010. Influence of oil well drilling waste on the engineering characteristics of clay bricks. Journal of American Science, *6*(7), pp.48-54.

Foroutan, M., Hassan, M.M., Desrosiers, N. and Rupnow, T., 2018. Evaluation of the reuse and recycling of drill cuttings in concrete applications. *Construction and Building Materials*, *164*, pp.400-409.

Gabr, M.H. and Uzawa, K., 2018. Mechanical, thermal, and interfacial shear properties of polyamide/nanoclay nanocomposites: study the effect of nanoclay on the micromechanism of fracture. *Journal of Thermoplastic Composite Materials*, *31*(4), pp.447-464.

Gendre, L., Njuguna, J., Abhyankar, H. and Ermini, V., 2015. Mechanical and impact performance of three-phase polyamide 6 nanocomposites. Materials & Design, 66, pp.486-491.

Holdway, D.A., 2002. The acute and chronic effects of wastes associated with offshore oil and gas production on temperate and tropical marine ecological processes. Marine Pollution Bulletin, 44(3), pp.185-203.

Huang, J.C., Zhu, Z.K., Yin, J., Qian, X.F. and Sun, Y.Y., 2001. Poly (etherimide)/montmorillonite nanocomposites prepared by melt intercalation: morphology, solvent resistance properties and thermal properties. Polymer, 42(3), pp.873-877.

Huskić, M. and Žigon, M., 2007. PMMA/MMT nanocomposites prepared by one-step in situ intercalative solution polymerization. European Polymer Journal, 43(12), pp.4891-4897.

Jahromi, A.E., Jahromi, H.R.E., Hemmati, F., Saeb, M.R., Goodarzi, V. and Formela, K., 2016. Morphology and mechanical properties of polyamide/clay nanocomposites toughened with NBR/NBR-g-GMA: a comparative study. *Composites Part B: Engineering*, *90*, pp.478-484.

Kalendová, A., Merinska, D., Gerard, J.F. and Slouf, M., 2013. Polymer/clay nanocomposites and their gas barrier properties. Polymer composites, 34(9), pp.1418-1424.

Kogbara, R.B., Ayotamuno, J.M., Onuomah, I., Ehio, V. and Damka, T.D., 2016. Stabilisation/solidification and bioaugmentation treatment of petroleum drill cuttings. Applied Geochemistry, 71, pp.1-8.

Lakshmi, M.S., Narmadha, B. and Reddy, B.S.R., 2008. Enhanced thermal stability and structural characteristics of different MMT-Clay/epoxy-nanocomposite materials. Polymer Degradation and Stability, 93(1), pp.201-213.

Leszczyńska, A., Njuguna, J., Pielichowski, K. and Banerjee, J.R., 2007a. Polymer/montmorillonite nanocomposites with improved thermal properties: Part I. Factors influencing thermal stability and mechanisms of thermal stability improvement. Thermochimica Acta, 453(2), pp.75-96.

Leszczyńska, A., Njuguna, J., Pielichowski, K., & Banerjee, J.R. 2007b. Polymer/montmorillonite nanocomposites with improved thermal properties: Part II. Thermal stability of montmorillonite nanocomposites based on different polymeric matrixes. Thermochimica Acta, 454(1), 1-22.

Li, S., Yuan, H., Yu, T., Yuan, W. and Ren, J., 2009. Flame-retardancy and anti-dripping effects of intumescent flame retardant incorporating montmorillonite on poly (lactic acid). Polymers for Advanced Technologies, 20(12), pp.1114-1120.

Liu, P., 2007. Polymer modified clay minerals: A review. Applied Clay Science, 38(1-2), pp.64-76.

Liu, S.P., Hwang, S.S., Yeh, J.M. and Hung, C.C., 2011. Mechanical properties of polyamide-6/montmorillonite nanocomposites—Prepared by the twin-screw extruder mixed technique. International communications in heat and mass transfer, 38(1), pp.37-43.

Liu, T.X., Liu, Z.H., Ma, K.X., Shen, L., Zeng, K.Y. and He, C.B., 2003. Morphology, thermal and mechanical behavior of polyamide 6/layered-silicate nanocomposites. *Composites science and technology*, *63*(3-4), pp.331-337.

Ma, J., Xu, J., Ren, J.H., Yu, Z.Z. and Mai, Y.W., 2003. A new approach to polymer/montmorillonite nanocomposites. Polymer, 44(16), pp.4619-4624.

Meera, K.M.S., Sankar, R.M., Murali, A., Jaisankar, S.N. and Mandal, A.B., 2012. Sol–gel network silica/modified montmorillonite clay hybrid nanocomposites for hydrophobic surface coatings. Colloids and Surfaces B: Biointerfaces, 90, pp.204-210.

Mishra, S., Shimpi, N.G. and Mali, A.D., 2012. Surface modification of montmorillonite (MMT) using column chromatography technique and its application in silicone rubber nanocomposites. Macromolecular Research, 20(1), pp.44-50.

Muschenheim, D.K. and Milligan, T.G., 1996. Flocculation and accumulation of fine drilling waste particulates on the Scotian Shelf (Canada). Marine Pollution Bulletin, (10).

Ormeloh, J., 2014. Thermomechanical cuttings cleaner–qualification for offshore treatment of oil contaminated cuttings on the Norwegian continental shelf and Martin Linge case study (Master's Thesis, University of Stavanger, Norway).

Pamukcu, S., Hijazi, M. and Fang, H., 1990. Study of possible reuse of stabilized petroleum contaminated soils as construction material. Petroleum Contaminated Soils, pp.203-14.

Priolo, M.A., Holder, K.M., Gamboa, D. and Grunlan, J.C., 2011. Influence of clay concentration on the gas barrier of clay–polymer nanobrick wall thin film assemblies. Langmuir, 27(19), pp.12106-12114.

Qin, H., Zhang, S., Zhao, C., Feng, M., Yang, M., Shu, Z. and Yang, S., 2004. Thermal stability and flammability of polypropylene/montmorillonite composites. Polymer Degradation and Stability, 85(2), pp.807-813.

Robinson, J.P., Kingman, S.W., Snape, C.E., Barranco, R., Shang, H., Bradley, M.S.A. and Bradshaw, S.M., 2009. Remediation of oil-contaminated drill cuttings using continuous microwave heating. Chemical Engineering Journal, 152(2-3), pp.458-463.

Sadiq, R. and Husain, T., 2005. A fuzzy-based methodology for an aggregative environmental risk assessment: a case study of drilling waste. Environmental Modelling & Software, 20(1), pp.33-46.

Sadiq, R., Husain, T., Veitch, B. and Bose, N., 2003. Marine water quality assessment of synthetic-based drilling waste discharges. International Journal of Environmental Studies, 60(4), pp.313-323.

Shah, K.J., Shukla, A.D., Shah, D.O. and Imae, T., 2016. Effect of organic modifiers on dispersion of organoclay in polymer nanocomposites to improve mechanical properties. Polymer, 97, pp.525-532.

Shishan, W., Dingjun, J., Xiaodong, O., Fen, W. and Jian, S., 2004. The structure and properties of PA6/MMT nanocomposites prepared by melt compounding. Polymer Engineering & Science, 44(11), pp.2070-2074.

Siddique, S., Kwoffie, L., Addae-Afoakwa, K., Yates, K. and Njuguna, J., 2017, May. Oil based drilling fluid waste: an overview on environmentally persistent pollutants. In IOP conference series: materials science and engineering (Vol. 195, No. 1, p. 012008). IOP Publishing.

Siddique, S., Kwoffie, L., Addae-Afoakwa, K., Yates, K. and Njuguna, J., 2019a. The crystallinity and thermal degradation behaviour of polyamide 6/Oil Based Mud Fillers (PA6/OBMFs) nanocomposites. Polymer degradation and stability, 159, pp.139-152.

Siddique, S., Smith, G.D., Yates, K., Mishra, A.K., Matthews, K., Csetenyi, L.J. and Njuguna, J., 2019b. Structural and thermal degradation behaviour of reclaimed clay nano-reinforced low-density polyethylene nanocomposites. Journal of Polymer Research, 26(6), p.154.

Siddique, S., Yates, K., Matthews, K., Csetenyi, L.J. and Njuguna, J., 2020c. Oil-based mud waste reclamation and utilisation in low-density polyethylene composites. *Waste Management & Research*, p.0734242X20941076.

Siddique, S., Yates, K. and Njuguna, J., Characterisation of oil based mud waste to explore the possibility in transforming waste into a value added product. Presented at the 6th International conference on sustainable solid waste management (NAXOS 2018), 13-16 June 2018, Naxos, Greece. Athens: National Technical University of Athens [online], paper number 45. Available from: http://uest.ntua.gr/nax...S2018_Siddique_etal.pdf.

Silva, F., Njuguna, J., Sachse, S., Pielichowski, K., Leszczynska, A. and Giacomelli, M., 2013. The influence of multiscale fillers reinforcement into impact resistance and energy absorption properties of polyamide 6 and polypropylene nanocomposite structures. Materials & Design, 50, pp.244-252.

Singla, P., Mehta, R. and Upadhyay, S.N., 2012. Clay modification by the use of organic cations. Green and sustainable chemistry, 2(1), pp.21-25.

Spínola, D.C., De Miranda, A., Macedo, D.A., Paskocimas, C.A. and Nascimento, R.M., 2019. Preparation of glass-ceramic materials using kaolin and oil well drilling wastes. *Journal of Materials Research and Technology*, *8*(4), pp.3459-3465.

Sun, L., Gibson, R.F., Gordaninejad, F. and Suhr, J., 2009. Energy absorption capability of nanocomposites: a review. Composites Science and Technology, 69(14), pp.2392-2409.

Thermtech, A., 2012. Thermomechanical Cuttings Cleaner (TCC): Setting the global Standard for the treatment of oily drill cuttings. 2006. Available at: http://www. thermtech. no. Accessed in: oct, 31.

Tjong, S.C. and Bao, S.P., 2004. Preparation and nonisothermal crystallization behavior of polyamide 6/montmorillonite nanocomposites. Journal of Polymer Science Part B: Polymer Physics, 42(15), pp.2878-2891.

Tjong, S.C., Meng, Y.Z. and Xu, Y., 2002. Structure and properties of polyamide-6/vermiculite nanocomposites prepared by direct melt compounding. Journal of Polymer Science Part B: Polymer Physics, 40(24), pp.2860-2870.

Tuncan, A., Tuncan, M. and Koyuncu, H., 2000. Use of petroleum-contaminated drilling wastes as sub-base material for road construction. Waste management & research, 18(5), pp.489-505.

Vazquez, A., López, M., Kortaberria, G., Martín, L. and Mondragon, I., 2008. Modification of montmorillonite with cationic surfactants. Thermal and chemical analysis including CEC determination. Applied Clay Science, 41(1-2), pp.24-36.

Wang, N., Cheng, K., Wu, H., Wang, C., Wang, Q. and Wang, F., 2012. Effect of nano-sized mesoporous silica MCM-41 and MMT on corrosion properties of epoxy coating. Progress in Organic Coatings, 75(4), pp.386-391.

Xi, Y., Frost, R.L., He, H., Kloprogge, T. and Bostrom, T., 2005. Modification of Wyoming montmorillonite surfaces using a cationic surfactant. Langmuir, 21(19), pp.8675-8680.

Xi, Y., Zhou, Q., Frost, R.L. and He, H., 2007. Thermal stability of octadecyltrimethylammonium bromide modified montmorillonite organoclay. Journal of Colloid and Interface Science, 311(2), pp.347-353.

Xie, W., Gao, Z., Liu, K., Pan, W.P., Vaia, R., Hunter, D. and Singh, A., 2001. Thermal characterization of organically modified montmorillonite. Thermochimica Acta, 367, pp.339-350.

Xu, T., Wang, X., Li, T. and Zhan, X., 2018. Heavy metal pollution of oil-based drill cuttings at a shale gas drilling field in Chongqing, China: A human health risk assessment for the workers. *Ecotoxicology and environmental safety*, *165*, pp.160-163.

Yu, Z.Z., Yan, C., Yang, M. and Mai, Y.W., 2004. Mechanical and dynamic mechanical properties of nylon 66/montmorillonite nanocomposites fabricated by melt compounding. Polymer International, 53(8), pp.1093-1098.

Zare, Y., Rhee, K.Y. and Park, S.J., 2019. A modeling methodology to investigate the effect of interfacial adhesion on the yield strength of MMT reinforced

nanocomposites. Journal of industrial and engineering chemistry, 69, pp.331-337.

Zheng, H., Zhang, Y., Peng, Z. and Zhang, Y., 2004. Influence of clay modification on the structure and mechanical properties of EPDM/montmo nanocomposites. Polymer Testing. 2004 Apr 1;23(2):217-23.

Caption of Figures

Fig. 1: SEM images of (a) OBMFs; (b) neat PA6; (c) PA6 with 2.5 wt% OBMFs; (d) PA6 with 5 wt% OBMFs; (e) PA6 with 7.5 wt% OBMFs; and (f) PA6 with 10 wt% OBMFs

Fig. 2: Tensile test samples before and after the test

Fig. 3: Young's modulus and tensile strength of neat PA6 and PA6/OBMFs nanocomposites with filler loading of 2.5, 5, 7.5 and 10 wt%

Fig. 4: Comparison of percentage elongation at yield of neat PA6 and OBMFs reinforced PA6 nanocomposites

Fig. 5: Flexural test sample presentation after the test

Fig. 6: Comparison of modulus of elasticity in bending and flexural strength of neat PA6 and OBMFs reinforced PA6/OBMFs nanocomposites with varying OBMFs concentrations

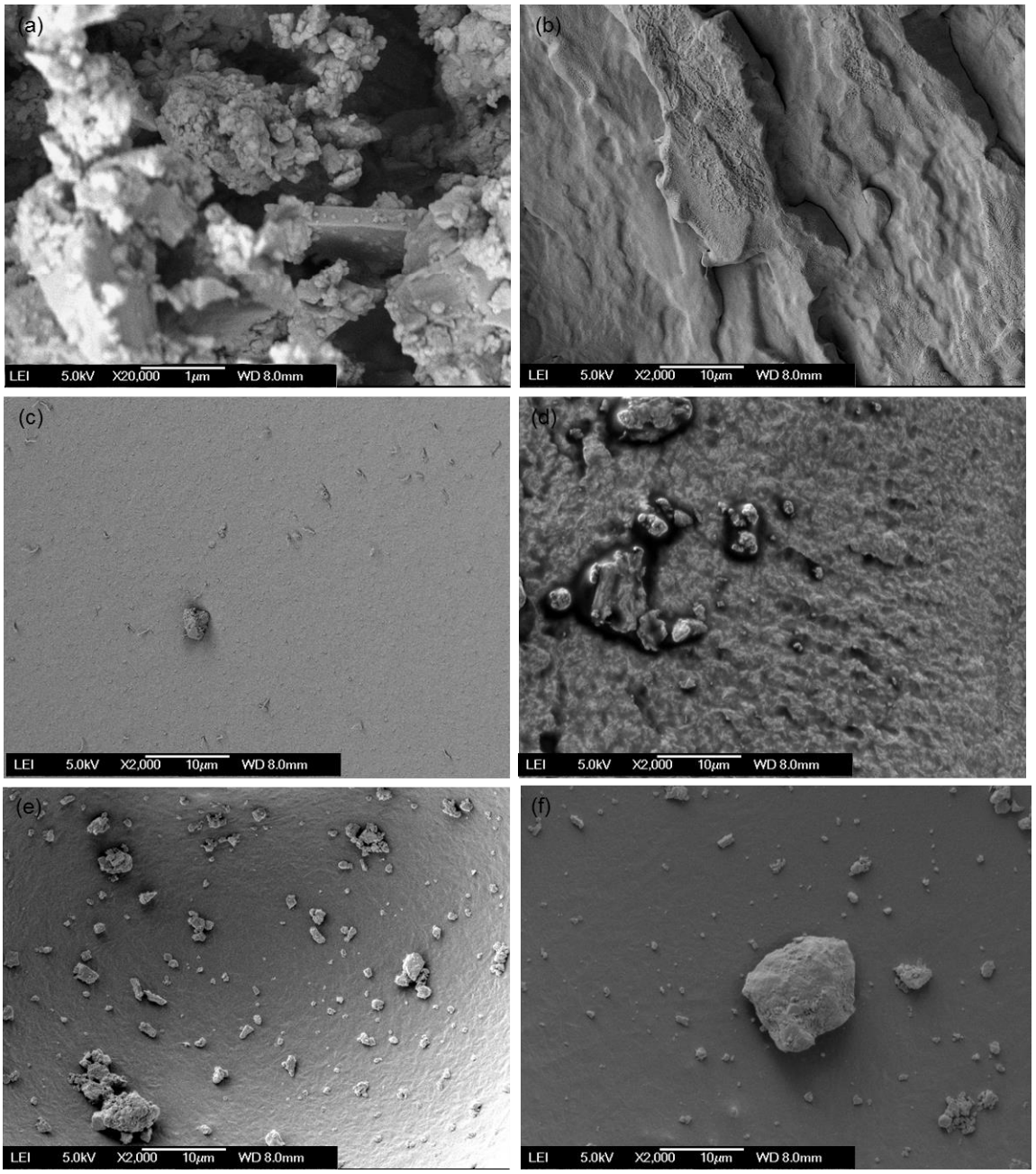

Fig. 1: SEM images of (a) OBMFs; (b) neat PA6; (c) PA6 with 2.5 wt% OBMFs; (d) PA6 with 5 wt% OBMFs; (e) PA6 with 7.5 wt% OBMFs; and (f) PA6 with 10 wt% OBMFs

Fig. 2: Tensile test samples before and after the test.

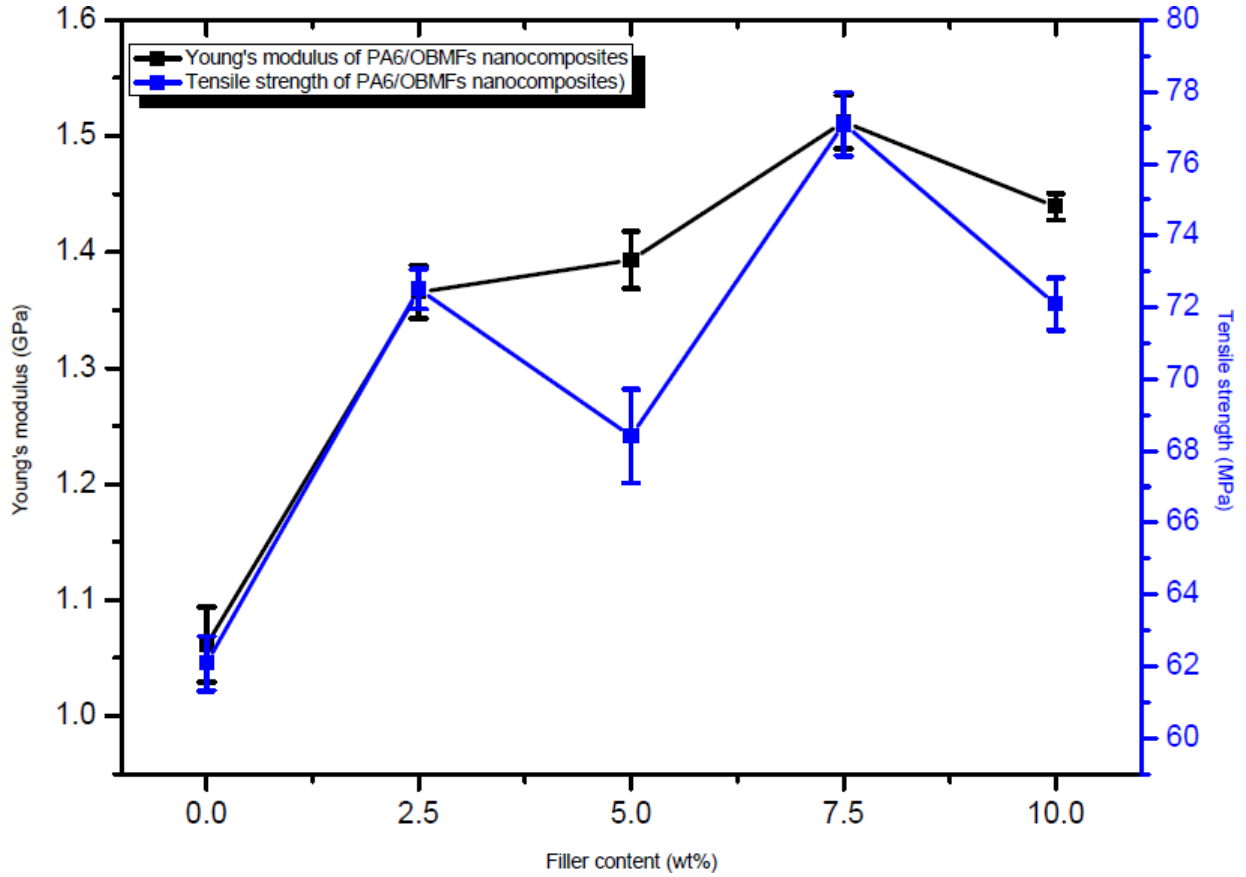

Fig. 3: Young's modulus and tensile strength of neat PA6 and PA6/OBMFs nanocomposites with filler loading of 2.5, 5, 7.5 and 10 wt%

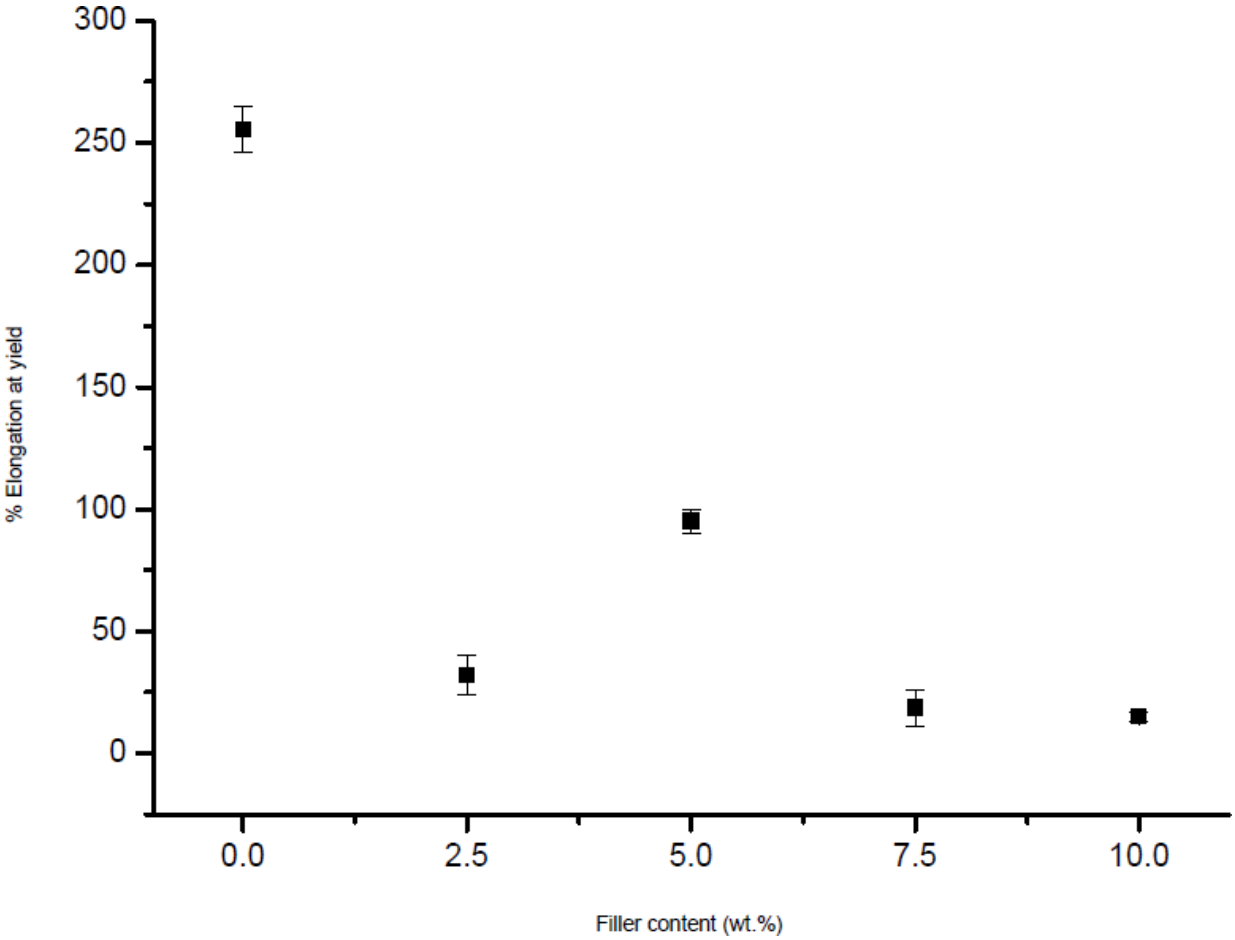

Fig. 4: Comparison of percentage elongation at yield of neat PA6 and OBMFs reinforced PA6 nanocomposites

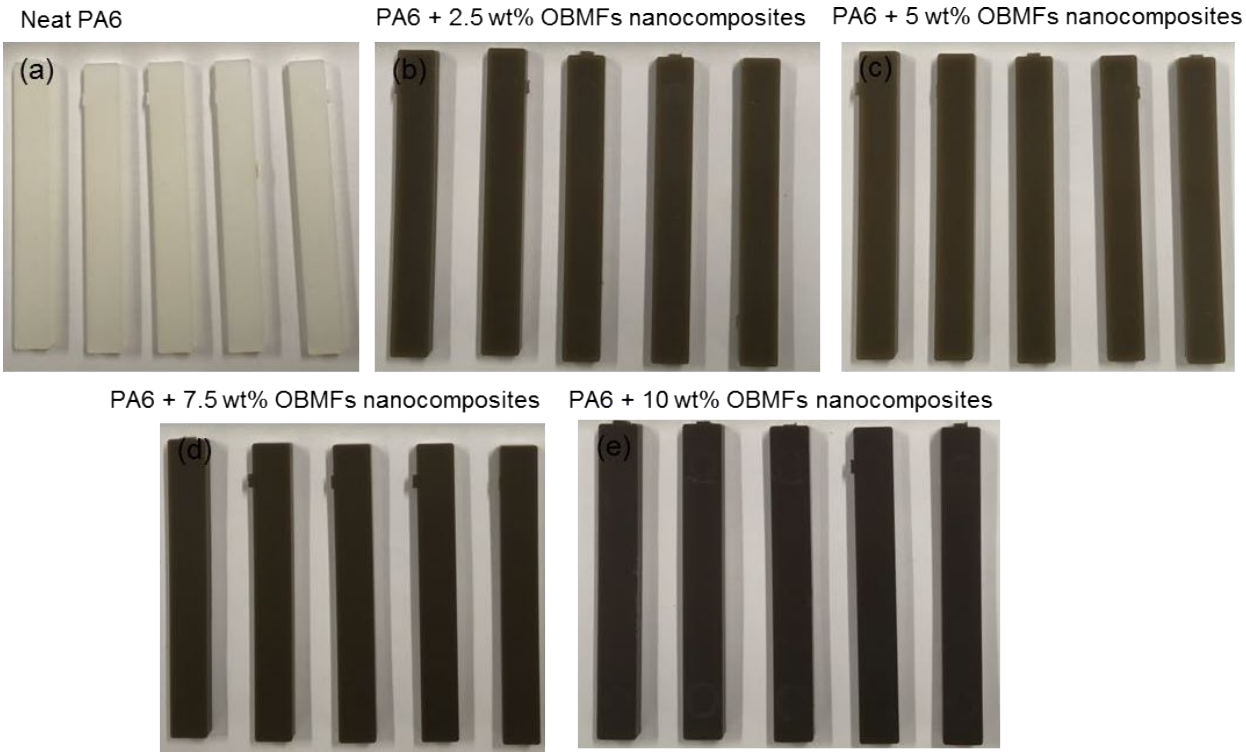

Fig. 5: Flexural test sample presentation after the test

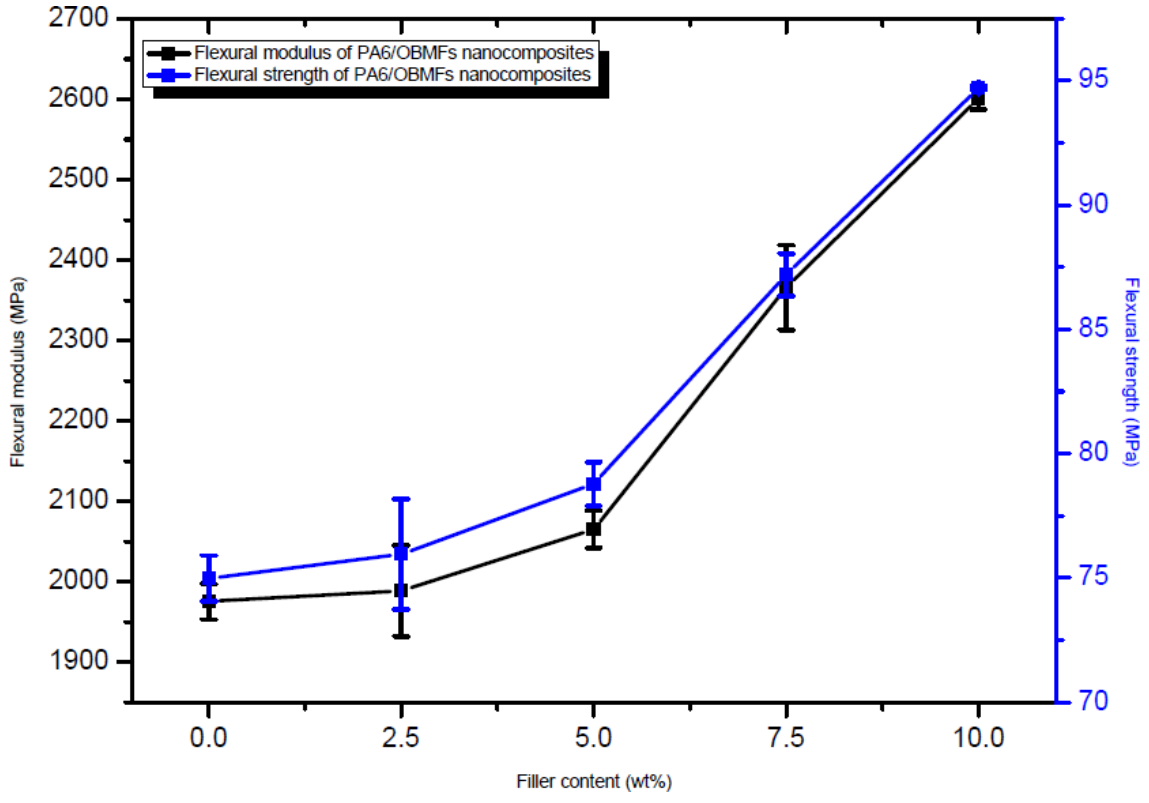

Fig. 6: Comparison of modulus of elasticity in bending and flexural strength of neat PA6 and OBMFs reinforced PA6/OBMFs nanocomposites with varying OBMFs concentrations

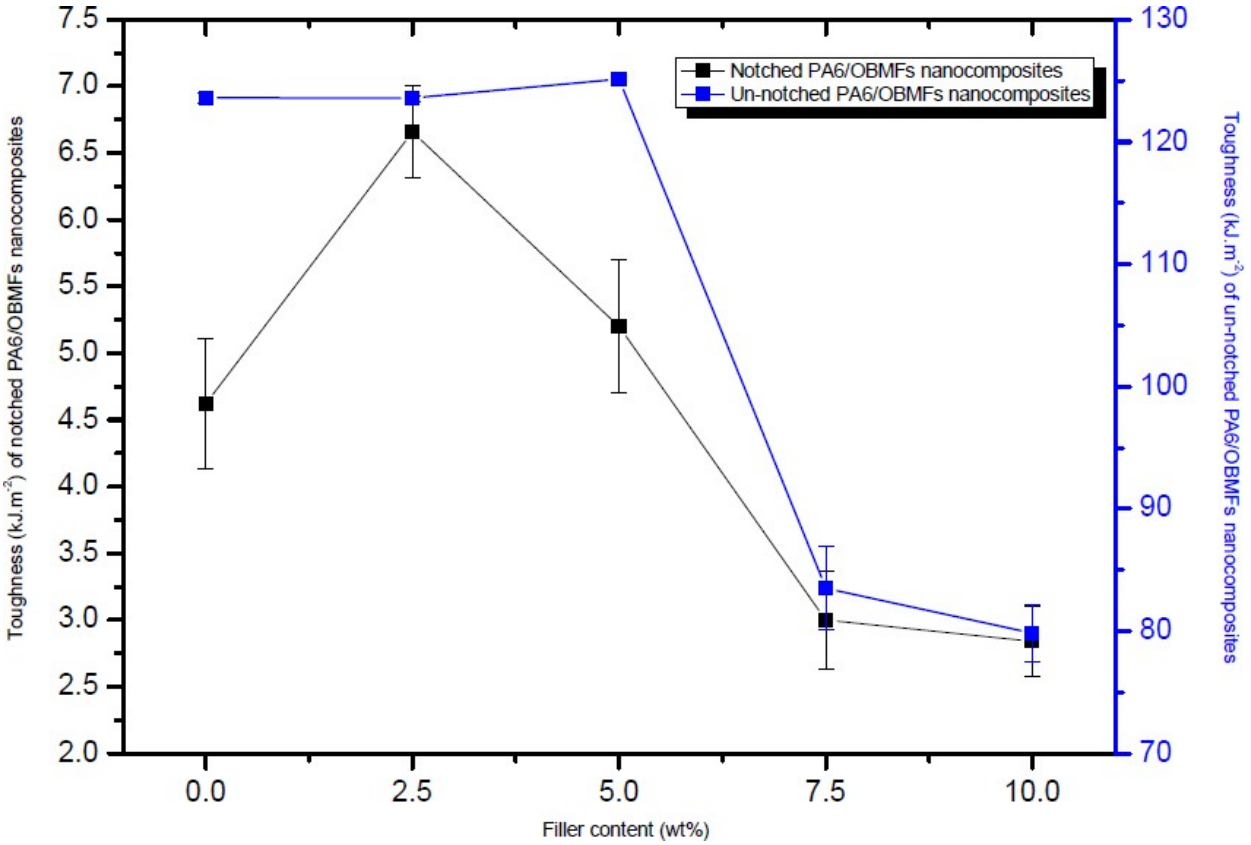

Fig. 7: Impact strength of both notched and un-notched neat PA6 and OBMFs reinforced PA6/OBMFs nanocomposites with varying OBMFs concentrations

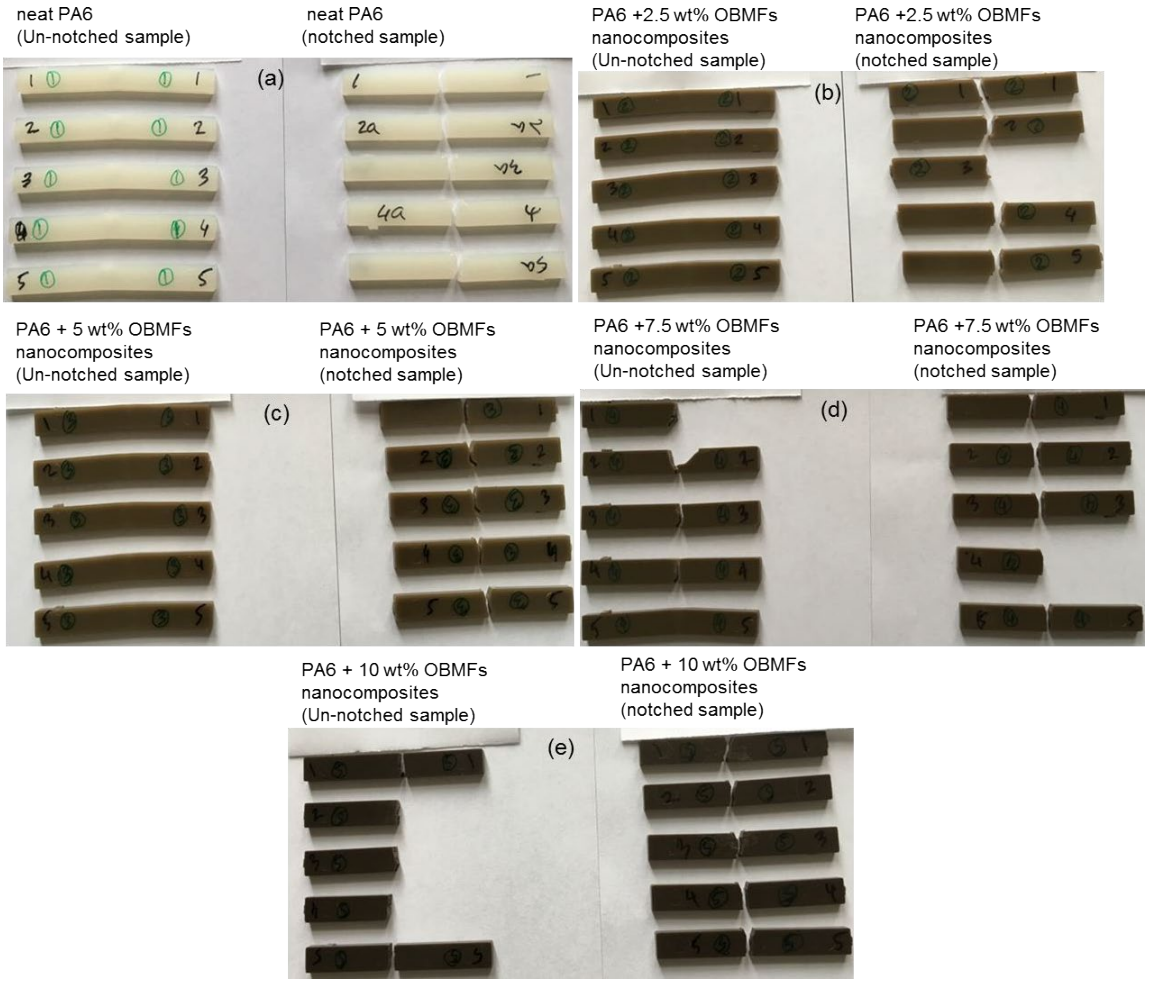

Fig. 8: Comparison and fracture analysis of Impact test samples

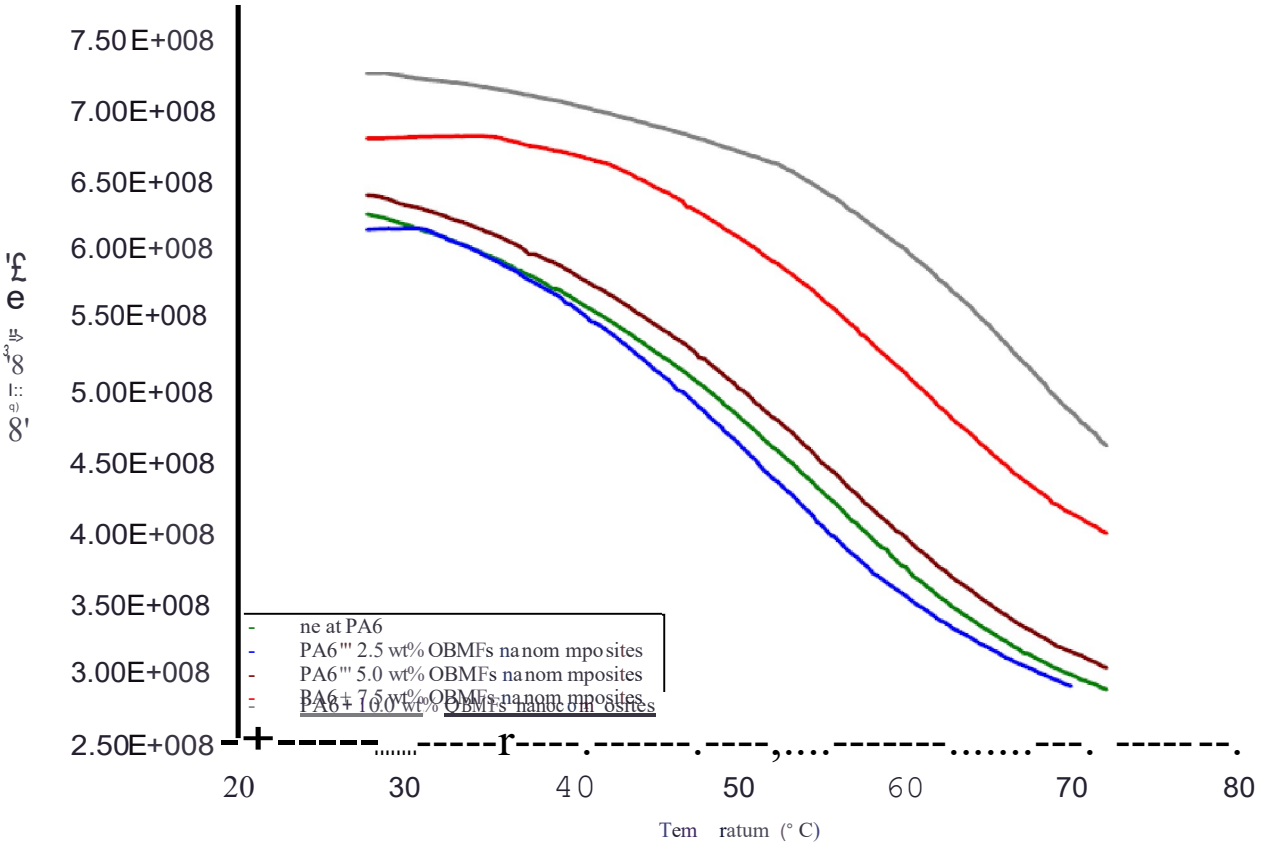
7.50E+008
7.00E+008
6.50E+008
6.00E+008
5.50E+008
5.00E+008
4.50E+008
4.00E+008
3.50E+008
3.00E+008
2.50E+008
20
30
40
50
60
70
80
ne at PA6
PA6 2.5 wt% OBMFs nanom mpo sites
PA6 5.0 wt% OBMFs nanom mposites
PA6 + 7.5 wt% OBMFs nanom mposites
PA6 + 10.0 wt% OBMFs nanocom osites
Tem ratum (° C)

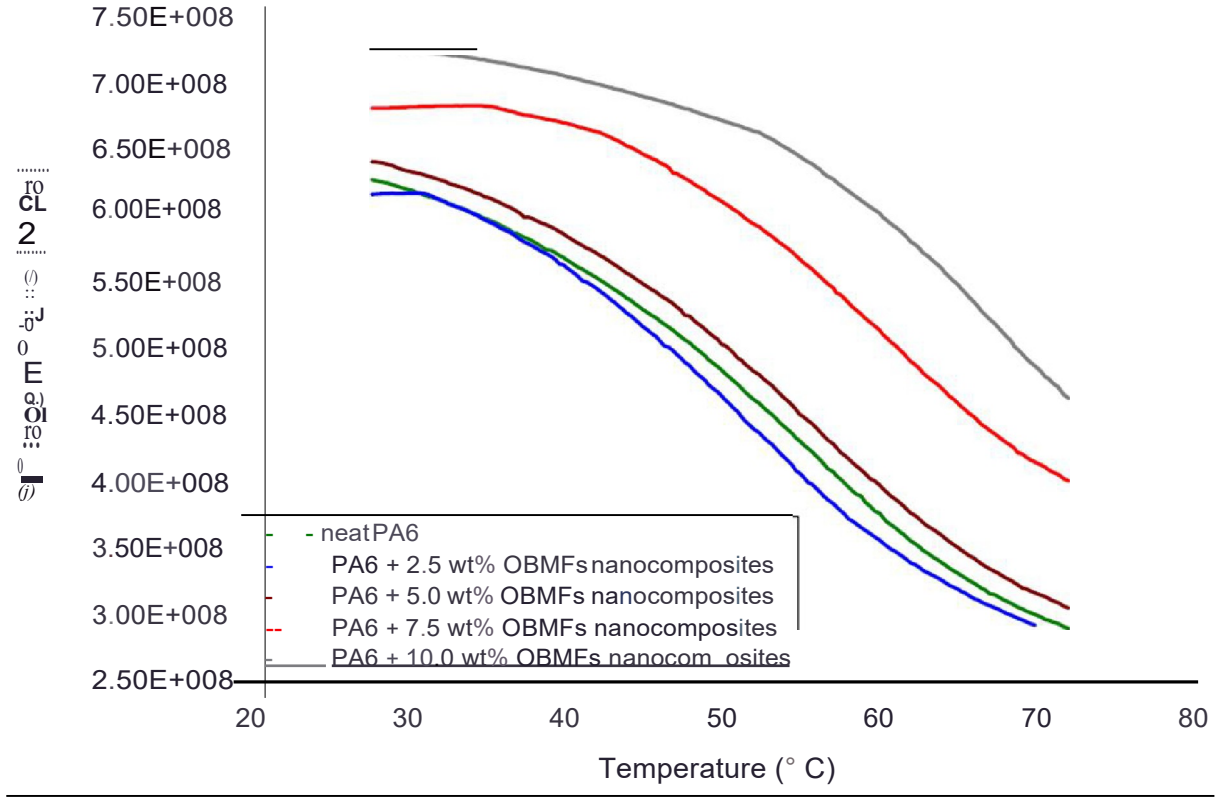
7.50E+008
7.00E+008
6.50E+008
6.00E+008
5.50E+008
5.00E+008
4.50E+008
4.00E+008
3.50E+008
3.00E+008
2.50E+008
20
30
40
50
60
70
80
- neat PA6
PA6 + 2.5 wt% OBMFs nanocomposites
PA6 + 5.0 wt% OBMFs nanocomposites
PA6 + 7.5 wt% OBMFs nanocomposites
PA6 + 10.0 wt% OBMFs nanocom osites
Temperature (° C)

Fig. 9: Dependence of storage modulus on temperature for neat PA6 and OBMFs reinforced PA6/OBMFs nanocomposites with varying OBMFs concentrations

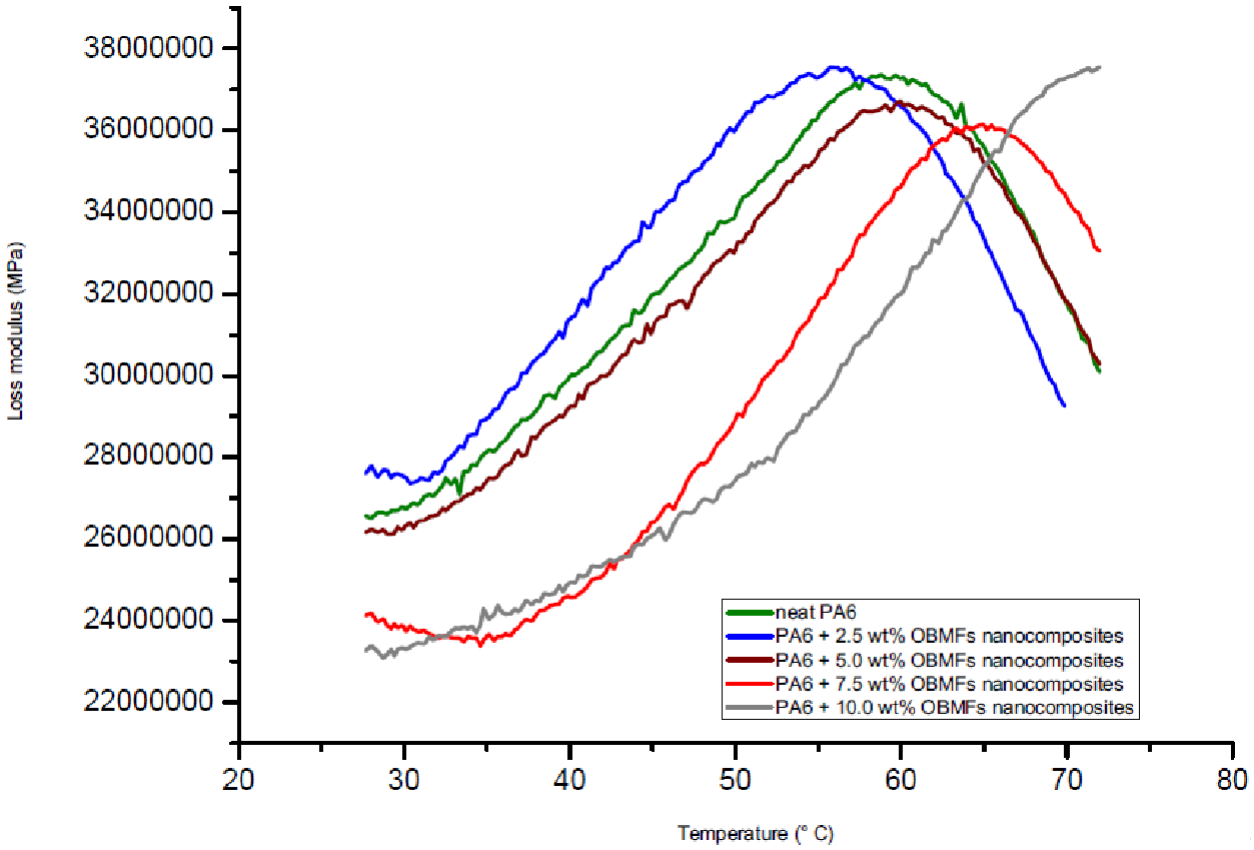

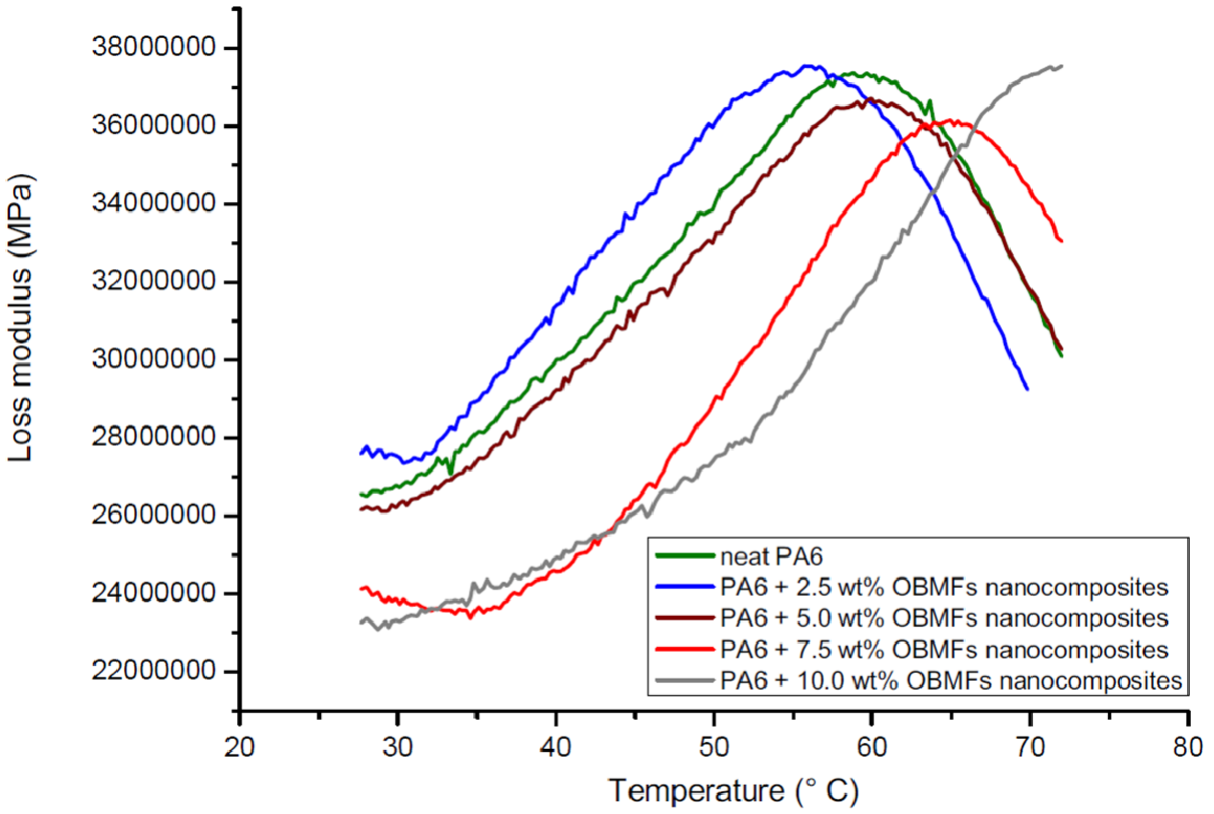

Fig. 10: Dependence of loss modulus on temperature for neat PA6 and OBMFs reinforced PA6/OBMFs nanocomposites with varying OBMFs concentrations

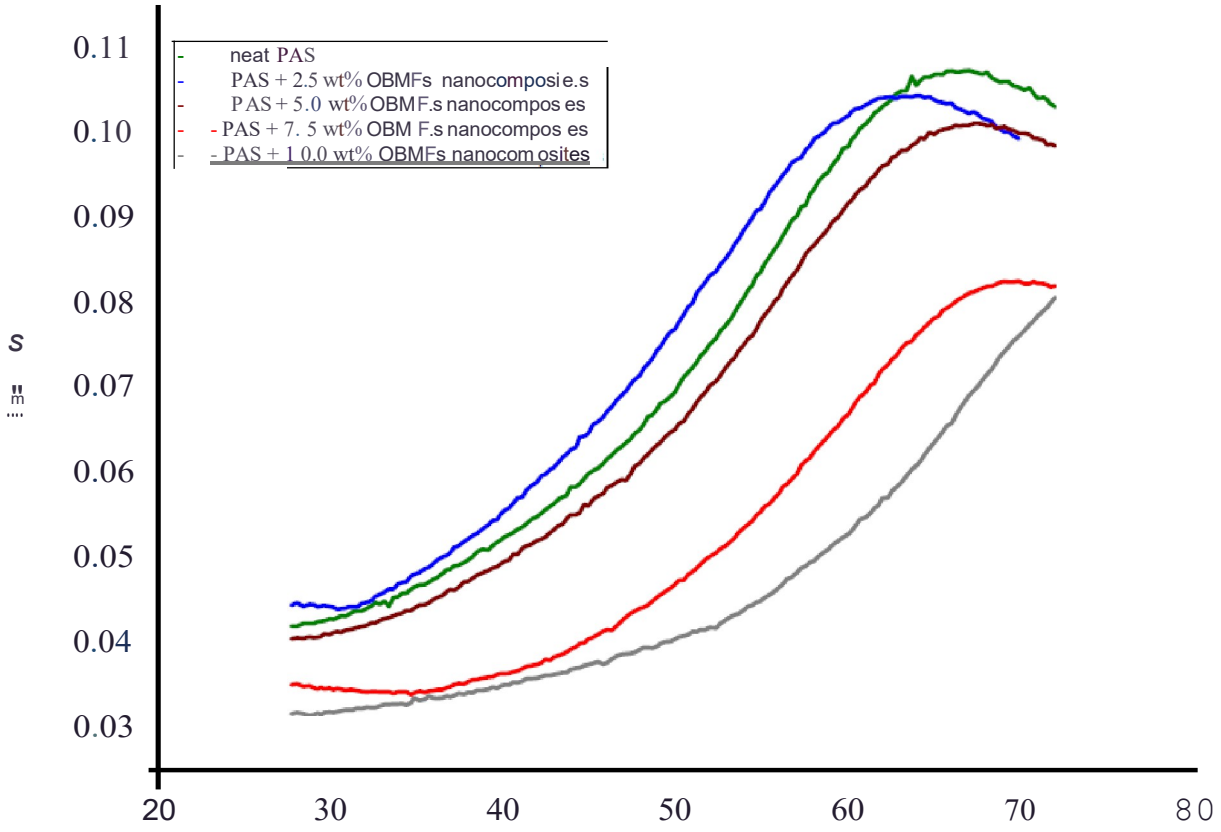
neat PAS
PAS + 2.5 wt% OBMFs nanocomposites
PAS + 5.0 wt% OBMFs nanocomposites
PAS + 7.5 wt% OBMFs nanocomposites
PAS + 10.0 wt% OBMFs nanocomposites
0.11
0.10
0.09
0.08
0.07
0.06
0.05
0.04
0.03
20
30
40
50
60
70
80
Temperature (° C)

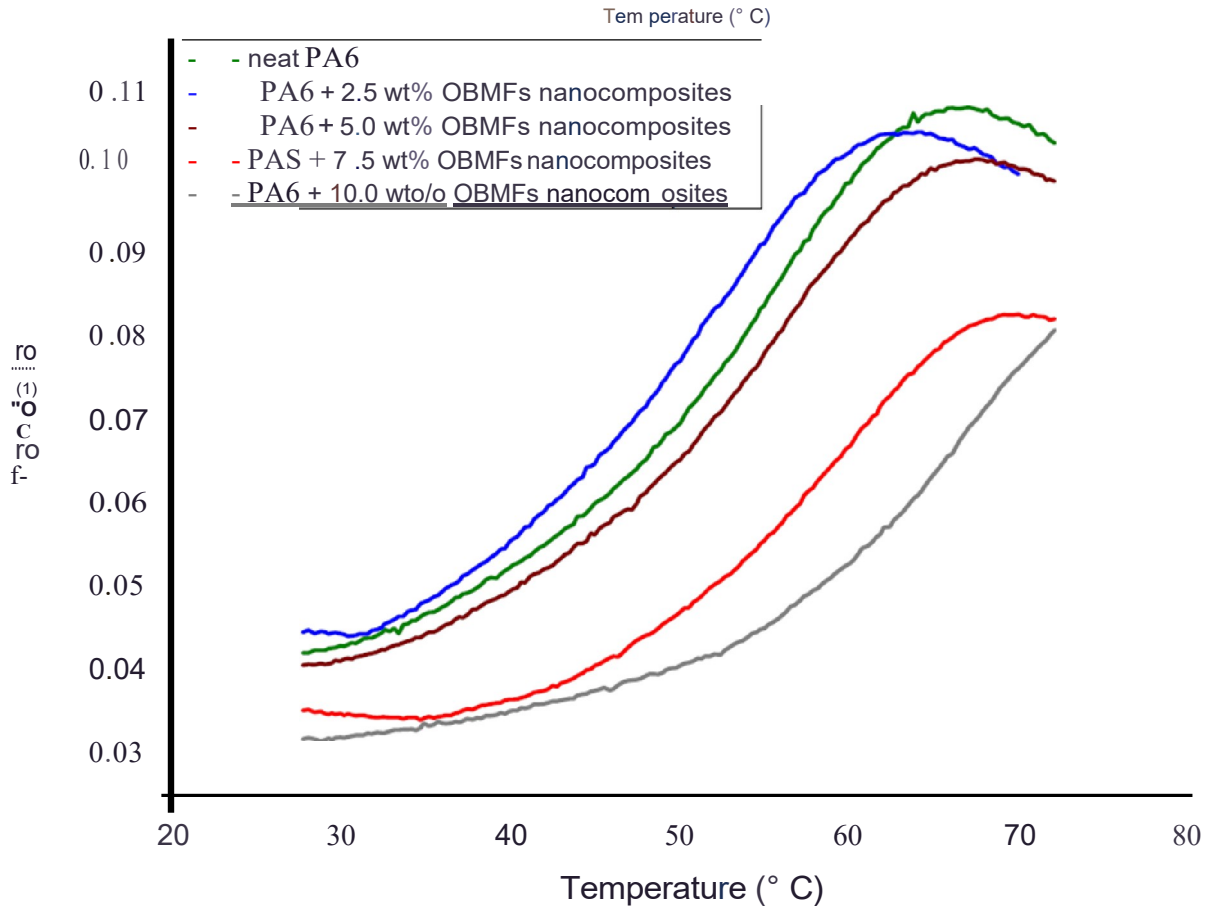
neat PA6
PA6 + 2.5 wt% OBMFs nanocomposites
PA6 + 5.0 wt% OBMFs nanocomposites
PAS + 7.5 wt% OBMFs nanocomposites
PA6 + 10.0 wto/o OBMFs nanocomposites
0.11
0.10
0.09
0.08
0.07
0.06
0.05
0.04
0.03
20
30
40
50
60
70
80
Temperature (° C)

Fig. 11: Dependence of loss factor (tan delta) on temperature for neat PA6 and OBMFs reinforced PA6/OBMFs nanocomposites with varying OBMFs concentrations

Drilling Oil-Based Mud Waste as a Resource for Raw Materials: A Case Study on Clays Reclamation and Their Application in Polyamide 6 Composites

Shohel Siddique[1], Pak Sing Leung[2] and James Njuguna[1*]

[1]Centre for Advanced Engineering Materials, School of Engineering, Robert Gordon University, Riverside East, Garthdee Road, Aberdeen, AB10 7GJ, UK

[2]Department of Mechanical and Construction Engineering, Northumbria University, Ellison Place, Newcastle upon Tyne, NE1 8ST, UK

[*]*Corresponding Author Email : j.njuguna@rgu.ac.uk; Tel. +44 (0) 1224262304*

Supplementary Information

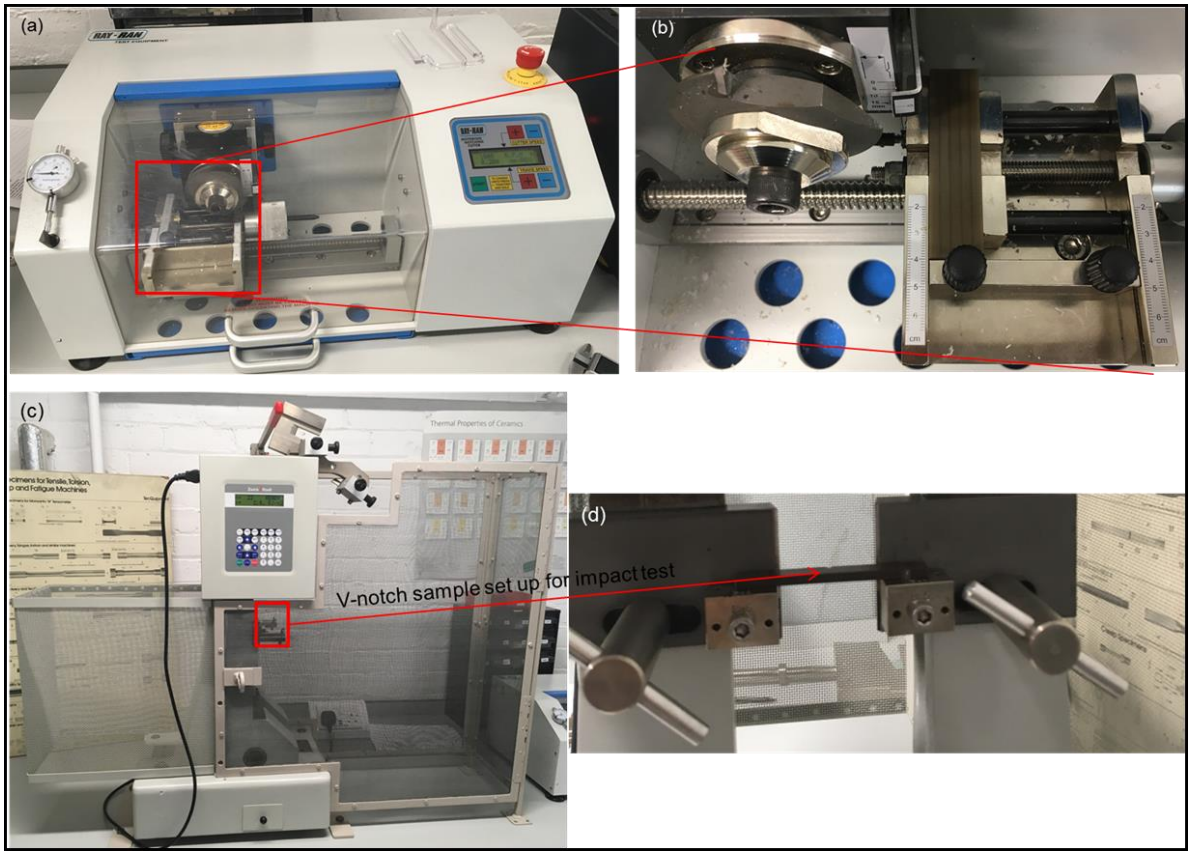

Fig. S1: V notch sample preparation (a) (b) and Impact test setting (c) (d)

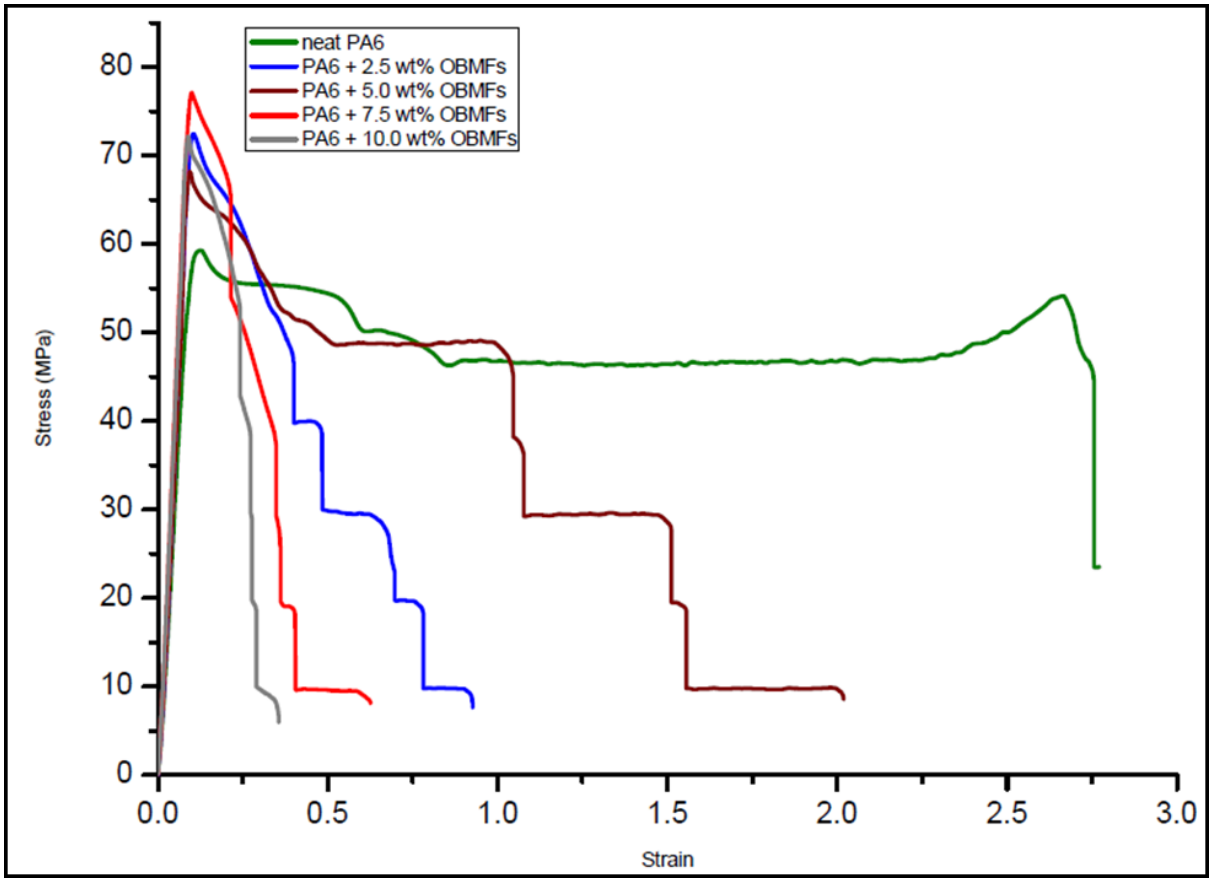

Fig. S2: Stress-strain curves of neat PA6 and PA6/OBMFs nanocomposites

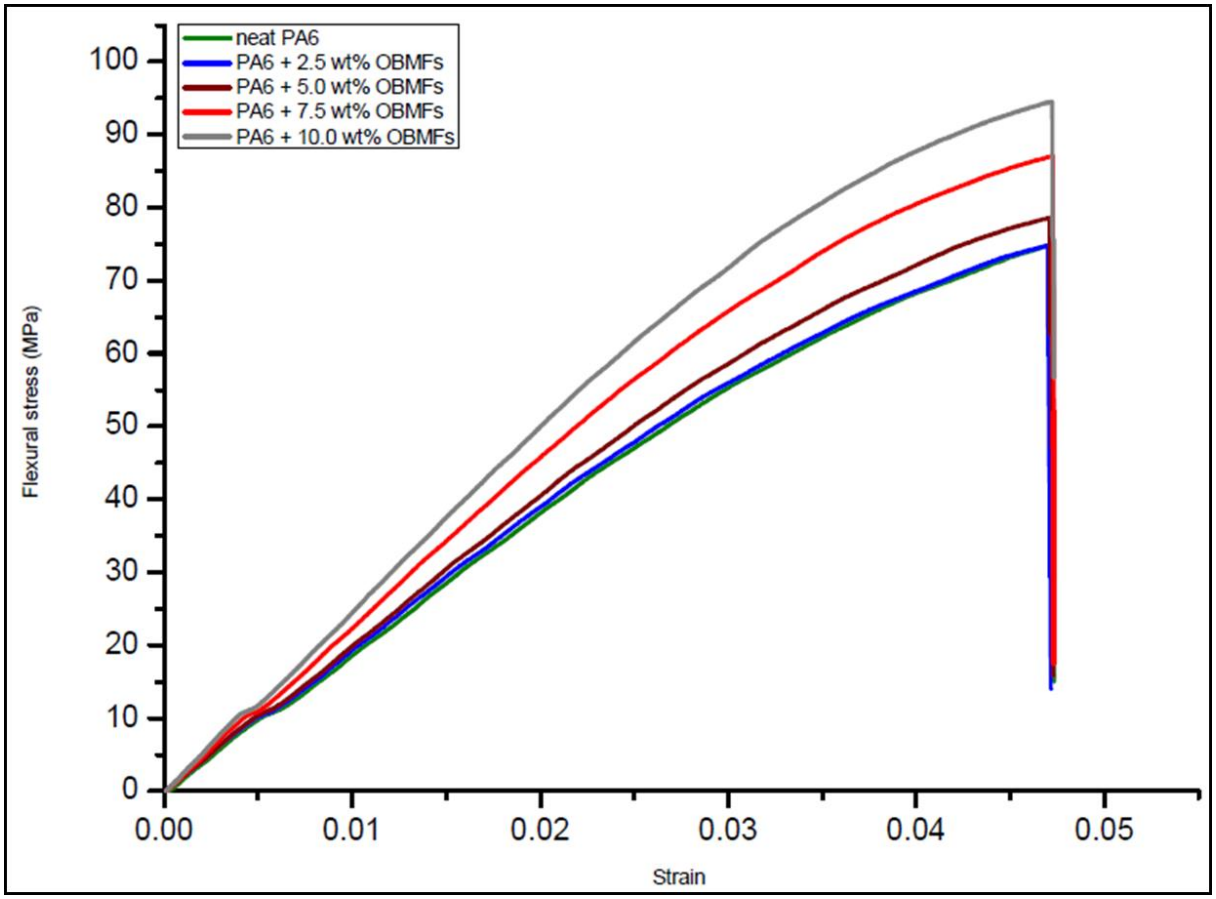

Fig. S3: Flexural stress-strain curve from 3-point bend test of neat PA6 and PA6/OBMFs nanocomposites with varying OBMFs concentrations